Strain Engineering of Plasma Dispersion Effect for SiGe Optical Modulators

Mitsuru Takenaka, *Member, IEEE*, and Shinichi Takagi, *Member, IEEE*

***Abstract*— The plasma dispersion effect and free-carrier absorption in strained SiGe are analyzed using the six-band $k \cdot p$ method and the Drude model. Since the hole conductivity mass of SiGe is decreased by applying compressive strain, enhancement of the plasma dispersion effect, and free-carrier absorption in strained SiGe is expected. We predict that $Si_{0.5}Ge_{0.5}$ coherently grown on Si will exhibit three times higher plasma dispersion and four times higher free-carrier absorption than Si. The modulation characteristics of SiGe quantum well metal-oxide-semiconductor (MOS) optical modulators are also analyzed by technology computer-aided design simulation and finite-difference optical mode analysis. An extremely small $V_\pi L$ of 0.033 V-cm is predicted in the case of a compressively strained $Si_{0.5}Ge_{0.5}$ quantum well in conjunction with a high-k gate dielectric MOS structure. The enhancement of free-carrier absorption in the SiGe high-k MOS modulator also makes in-line intensity modulation feasible and an intensity modulation efficiency of 9 dB/mm/V is predicted.**

***Index Terms*— High-k dielectric, metal-oxide-semiconductor, optical modulator, Si photonics, SiGe quantum well, strain engineering.**

I. Introduction

SILICON-based optical modulators for optical communication systems have significantly developed [1] since the first demonstration of a silicon (Si) modulator capable of operating at speeds exceeding 1 GHz in 2004 [2]. Although many attempts to explore new modulation mechanisms such as the Franz-Keldysh effect [3] and the quantum-confined Stark effect (QCSE) [4] with the aim of overcoming the weak Pockels effect and Kerr effect in Si at the telecommunication wavelength range from 1.3 μm to 1.55 μm have been reported [5], the most common method of achieving modulation in Si is to employ the plasma dispersion effect, which was quantitatively evaluated by Soref and Bennett [5]. The change in refractive index induced by the plasma dispersion effect is obtained through change in carrier density resulting from carrier injection, depletion, and accumulation.

Manuscript received July 26, 2011; revised October 4, 2011; accepted November 6, 2011. Date of current version November 25, 2011. This work was supported in part by the Strategic Information and Communications Research and Development Promotion Programme of the Ministry of Internal Affairs and Communications.

M. Takenaka is with the Department of Electrical Engineering and Information Systems, University of Tokyo, Tokyo 113-8656, Japan. He is also with PRESTO, Japan Science and Technology Agency, Saitama 332-0012, Japan (e-mail: takenaka@mosfet.t.u-tokyo.ac.jp).

S. Takagi is with the Department of Electrical Engineering and Information Systems, University of Tokyo, Tokyo 113-8656, Japan (e-mail: takagi@ee.t.u-tokyo.ac.jp.

Color versions of one or more of the figures in this paper are available online at http://ieeexplore.ieee.org.

Digital Object Identifier 10.1109/JQE.2011.2176104

Mach-Zehnder interferometer (MZI)-based Si optical modulators have been demonstrated by using carrier depletion in a p-n junction [6]-[11] or the carrier accumulation in a metal-oxide-semiconductor (MOS) structure [2], [12], [13]. The fast response of the majority carriers enables an operation speed of up to 40 GHz [8], [11]. However the figure of merit for phase modulation efficiency, $V_\pi L$ (where V_π is the driving voltage required for a phase shift of π and L is the device length) is typically 1 V-cm [10] to 4 V-cm [7], resulting in a device length of more than 1 mm for MZI-based modulators. Although the ring-resonator-based modulators can reduce the device footprint to less than 200 μm^2 [14], the optical bandwidth of the ring modulators is also reduced from more than 20 nm in the case of MZI-based modulators to 0.1 nm, which results in high sensitivity to variations in temperature and fabrication conditions. Carrier injection enables greater modulation of free-carrier density than carrier depletion, and ring-based modulators [15, 16] and an MZI-based modulator [17] with high modulation efficiencies have been demonstrated. High-speed operation with a frequency of up to 12.5 GHz has been demonstrated [16]. However, carrier-injection-based modulators are limited by long minority carrier lifetimes, and faster modulation will be difficult without the additional power consumption for a pre-emphasis electrical drive signal. Hence, enhancement of the plasma dispersion effect will be required to achieve higher-performance Si-based optical modulators regardless of the carrier modulation mechanism.

In this paper, we evaluate the enhancement of plasma dispersion effect and free-carrier absorption in strained silicon germanium (SiGe) using the 6-band $k \cdot p$ method and the Drude model. We predict that the application of compressive strain to SiGe will reduce the hole conductivity mass, resulting in enhanced plasma dispersion effect and free-carrier absorption. In the case of compressively strained $Si_{0.5}Ge_{0.5}$ coherently grown on Si, three times higher plasma dispersion effect and four times higher free-carrier absorption than those of Si are predicted. We also analyze the modulation characteristics of MOS-based compressively strained SiGe quantum well (QW) optical modulators by technology computer-aided design (TCAD) in conjunction with a finite-difference mode solver for optical waveguides. We predict that a $Si_{0.5}Ge_{0.5}$ modulator with a high-k gate dielectric MOS structure will exhibit an extremely small $V_\pi L$ of 0.033 V-cm. The enhancement of free-carrier absorption in strained SiGe will also enable the realization of an in-line intensity modulator, which has a much simpler structure than MZI modulators. The

TABLE I
MATERIAL PARAMETERS OF Si AND Ge

Symbol	Quantity	Units	Si	Ge
a	lattice constant	Å	5.43	5.65
C_{11}	elastic constants	Mbar	1.658	1.285
C_{12}		Mbar	0.539	0.483
a_v	hydrostatic deformation potential	eV	2.46	1.24
b	Bir-Pikus shear deformation potential	eV	−2.2	−2.3
d		eV	−5.1	−5.0
Δ	spin-orbit split-off energy	eV	0.044	0.295
L	valence band parameters	$\hbar/2m_0$	−5.53	−30.53
M			−3.64	−4.64
N			−8.32	−33.64

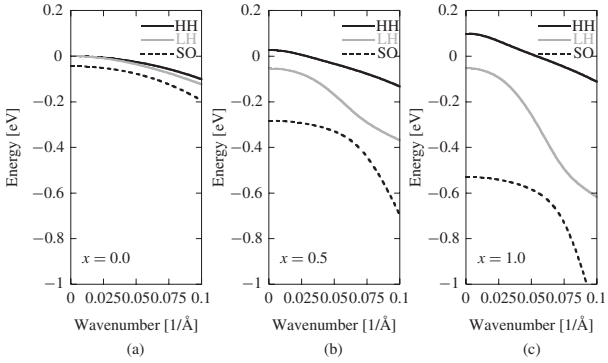

Fig. 1. Valence band structures of $Si_{1-x}Ge_x$ grown on (100) Si as a function of wavenumber along the in-plane [100] direction calculated by the six-band $k\cdot p$ method. (a) Si. (b) $Si_{0.5}Ge_{0.5}$. (c) Ge. Black solid curves: heavy hole (HH) bands, gray solid curves: the light hole (LH) bands, dashed curves: spin-orbit split-off (SO) bands.

intensity modulation efficiency of a $Si_{0.5}Ge_{0.5}$ high-k MOS modulator is predicted to be 9 dB/mm/V.

The paper is organized as follows: In Section II we describe the plasma dispersion effect and free-carrier absorption of strained SiGe; in Section III we report the modulation characteristics of SiGe QW high-k MOS optical modulators; and conclusions are given in Section IV.

II. EFFECT OF STRAIN ON PLASMA DISPERSION EFFECT AND FREE-CARRIER ABSORPTION OF SiGe

The lattice constant of SiGe is larger than that of Si; thus, a SiGe film coherently grown on Si contains biaxial compressive strain when the SiGe thickness is less than its critical thickness [18]. The band structure of strained SiGe strongly depends on the strain [19], and the hole conductivity mass is markedly reduced by compressive strain. Enhancement of the plasma dispersion effect and free-carrier absorption through the reduction of the hole conductivity mass is analyzed by the Drude model and valence band calculation through the 6-band $k\cdot p$ method.

A. Drude Model

The plasma dispersion effect and free-carrier absorption can be approximately expressed by the Drude model. The well-known formulas for the changes in refractive index (Δn) and absorption ($\Delta\alpha$) due to changes in free electron density (ΔN_e) and free hole density (ΔN_h) are as follows [5]:

$$\Delta n = -\left(e^2\lambda^2/8\pi^2c^2\varepsilon_0 n\right)\left[\Delta N_e/m_{ce}^* + \Delta N_h/m_{ch}^*\right] \quad (1)$$

$$\Delta\alpha = \left(e^3\lambda^2/4\pi^2c^3\varepsilon_0 n\right)\left[\Delta N_e/{m_{ce}^*}^2\mu_e + \Delta N_h/{m_{ch}^*}^2\mu_h\right] \quad (2)$$

where e is the elementary charge, ε_0 is the permittivity in vacuum, c is the speed of light in vacuum, λ is the wavelength, n is the unperturbed refractive index, m_{ce}^* is the conductivity effective mass of electrons, m_{ch}^* is the conductivity effective mass of holes, μ_e is the electron mobility, and μ_h is the hole mobility. According to the Drude model, the change in refractive index through the plasma dispersion effect is proportional to $1/m_{ce}^*$ and $1/m_{ch}^*$; thus, the modulation of the conductivity effective mass by the application of strain is effective for enhancing the plasma dispersion effect. In the case of free-carrier absorption, the change in the absorption depends on not only the effective mass but also the mobility. Therefore, when evaluating the free-carrier absorption, it is important to take the mobility in strained SiGe into account in addition to the effective mass.

B. Hole Conductivity Mass of Strained SiGe

The valence band structure of strained SiGe is calculated by the $k\cdot p$ method [20], [21]. The 6×6 Luttinger-Kohn Hamiltonian of biaxially strained SiGe on Si is solved to evaluate strain-induced coupling between the heavy-hole (HH) bands, light-hole (LH) bands, and the spin-orbit split-off (SO) bands [22]. Table I shows material parameters of Si and Ge employed in this paper. All values are from [23], [24] except for the valence band parameters [25]. The unit of the valence band parameters is $\hbar/2m_0$, where $\hbar$ is the reduced Planck constant and m_0 is the electron mass. The values for SiGe are obtained by linear interpolation of those for Si and Ge, with the exception of the lattice constant of $Si_{1-x}Ge_x$, which is approximately expressed as

$$a_{SiGe}(x) = a_{Si} + 0.200326\cdot x(1-x) + (a_{Ge} - a_{Si})\ x^2 \quad (3)$$

where x is the Ge mole fraction [26].

Figure 1 shows the valence band structures of compressively strained $Si_{1-x}Ge_x$ grown on a (100) Si substrate as a function of wavenumber k along the in-plane [100] direction. In the case of Si ($x = 0$), the HH band and LH band are degenerate at the Γ point ($k = 0$). The compressive strain splits this degeneracy; thus, the HH band is shifted to above the LH band in the case of strained $Si_{1-x}Ge_x$ on Si ($x > 0$). Figure 2 shows the in-plane hole conductivity mass of SiGe as a function of Ge mole fraction obtained from the band structure results. The hole conductivity masses of $Si_{1-x}Ge_x$ ($x > 0$) are calculated from the curvatures at the minimum HH band edges. In the case of Si, the degeneracy of the HH and LH bands is included when calculating the conductivity mass [27]. As shown in Fig. 2, the hole conductivity mass of SiGe decreases with increasing Ge fraction owing to high compressive strain.

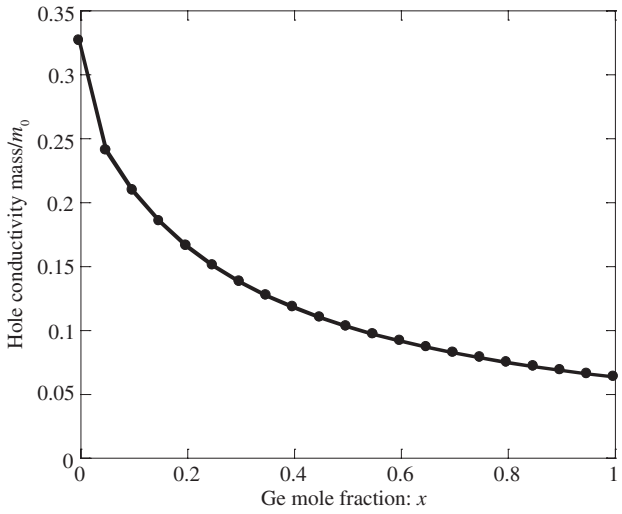

Fig. 2. Calculated in-plane hole conductivity masses of compressively strained $Si_{1-x}Ge_x$ grown on (100) Si.

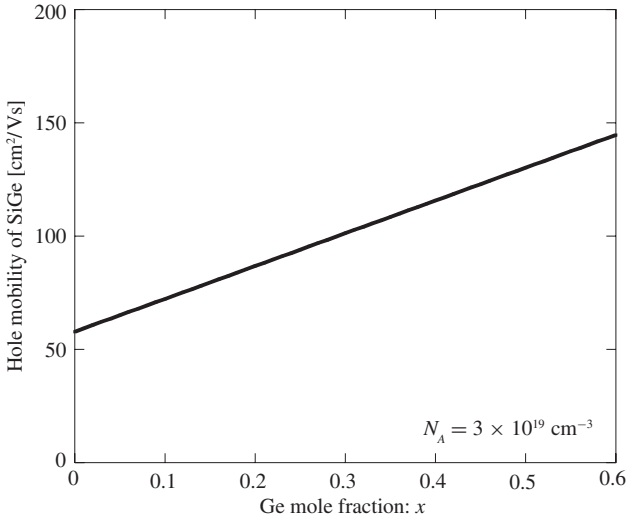

Fig. 3. Calculated hole mobility of compressively strained $Si_{1-x}Ge_x$ grown on (100) Si when $N_A = 3 \times 10^{19}$ cm^{-3}.

The hole conductivity mass of $Si_{0.5}Ge_{0.5}$ is approximately three times smaller than that of Si.

C. Hole Mobility of Strained SiGe

The hole mobility of strained SiGe (μ_{SiGe}) was theoretically and experimentally investigated by Manku et al. [28]. In the case of a Ge fraction of less than 0.2, the hole mobility of compressively strained $Si_{1-x}Ge_x$ on Si is approximately expressed as

$$\mu_{SiGe}(x) = \mu_{Si}(2.5x + 1) \tag{4}$$

where μ_{Si} is the Si hole mobility. This relationship has been found to be valid regardless of the doping level. The calculated hole mobility of SiGe when the Ge fraction exceeds 0.2 is reported in [25]. However, the calculated hole mobility is strongly dependent on the value assumed for the alloy interaction potential and might be lower than experimental values. Thus, we assume relationship (4) for $Si_{1-x}Ge_x$ with $x > 0.2$, and the hole mobility is calculated by extrapolating (4).

The room-temperature Si hole mobility [cm^2/Vs] is given by the well-established formula [29]

$$\mu_{Si}(N_A) = 54.3 + 406.9 \Big/ \left[1 + \left(N_A/2.35 \times 10^{17}\right) \cdot 0.88\right] \tag{5}$$

where N_A [cm^{-3}] is the acceptor concentration. Figure 3 shows the calculated hole mobility of $Si_{1-x}Ge_x$ on Si obtained using (4) and (5). Although the hole mobility was expected to be proportional to $1/m^*_{ch}$, the enhancement in the hole mobility is slightly lower than the expected value because of the alloy scattering in SiGe as discussed in [28].

D. Energy Gap of Strained SiGe

The energy gap of strained SiGe on Si experimentally investigated by Lang et al. [30] is shown in Fig. 4. The dotted line shows the analytical expression obtained by Robbins [31], which is given by

$$E_{SiGe}(x) = 1.155 - 0.874x + 0.376x^2. \tag{6}$$

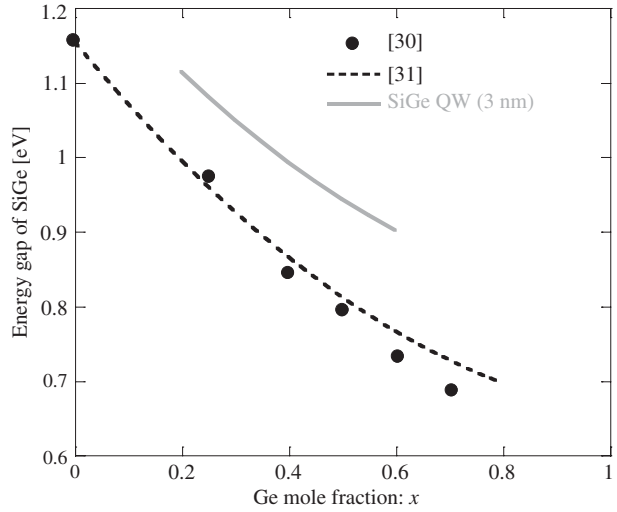

Fig. 4. Energy gap of compressively strained $Si_{1-x}Ge_x$ grown on (100) Si.

Although (6) was obtained for $x < 0.24$, the energy gap was well fitted to the experimental value for a Ge mole fraction of up to 0.6. As shown in Fig. 4, the energy gap of SiGe grown on Si is decreased by the compressive strain. To avoid bandgap absorption at a wavelength of 1.55-μm, the energy gap of SiGe should be larger than approximately 0.9 eV. In the case of bulk SiGe, the Ge mole fraction should be less than approximately 0.3 for optical modulator application at this wavelength. In the case of a QW structure, the energy gap is increased by the quantized energy. We calculated the quantized energy using out-of-plane effective masses obtained by the $k \cdot p$ method described in [22]. The solid line in Fig. 4 shows the energy gap of a 3-nm-thick SiGe QW calculated from the obtained quantized energy and the bulk SiGe energy gap expressed by (6). The quantized energy is approximately 0.12–0.13 eV; thus, the SiGe with x up to approximately 0.5 can be used in an optical modulator at a wavelength of 1.55-μm when the QW is used.

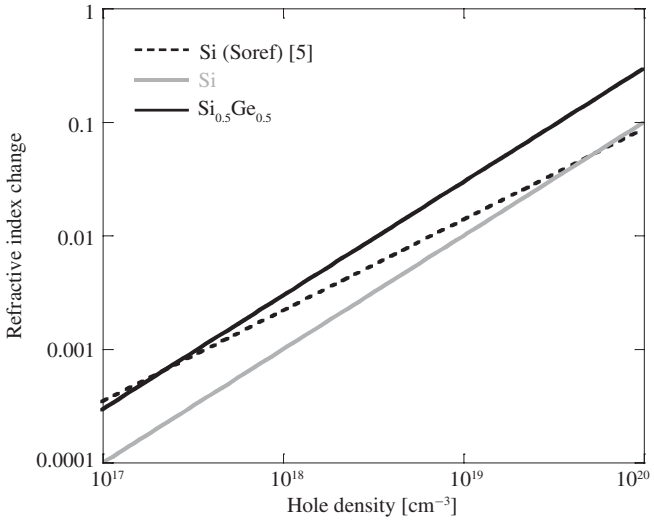

Fig. 5. Changes in refractive index of compressively strained SiGe and Si calculated by the Drude model. The result for Si obtained from the Soref's model is also plotted as a dotted line.

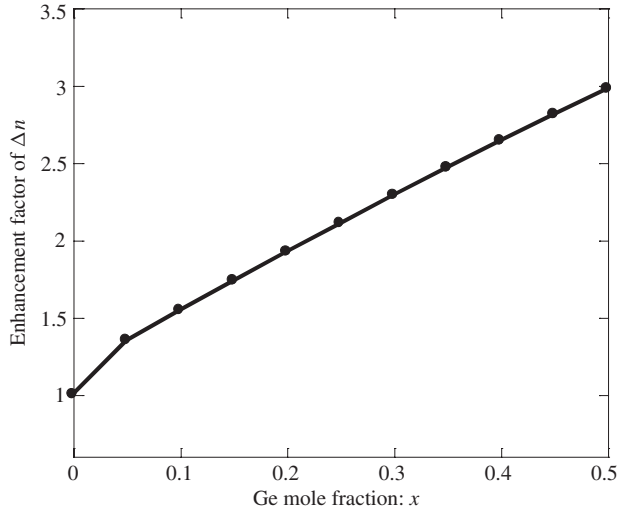

Fig. 6. Enhancement factor of the changes in the refractive index of compressively strained SiGe relative to that of Si as a function of Ge mole fraction.

E. Plasma Dispersion and Free-Carrier Absorption in SiGe

The plasma dispersion effect and free-carrier absorption at 1.55 μm induced by holes in compressively strained SiGe are calculated by the Drude model in conjunction with the hole conductivity mass shown in Fig. 2. The refractive index of SiGe is taken from [32]. The calculated changes in the refractive index of $Si_{0.5}Ge_{0.5}$ and Si as a function of hole density are shown in Fig. 5. In the calculation of the plasma dispersion effect and free-carrier absorption, only the in-plane effective mass and mobility are taken into account because we only consider the transverse electric (TE) mode, which mainly has an in-plane electric field. For comparison, we also plot the change in the refractive index of Si obtained by Soref and Bennett [5], which is expressed by

$$\Delta n = -\left(8.8 \times 10^{-22}\Delta N_e + 8.5 \times 10^{-18}\left(\Delta N_h\right)^{0.8}\right). \quad (7)$$

Although the change in the refractive index is not proportional to the hole density as in Fig. 5 in the Soref's model, the change in the refractive index of Si calculated by the Drude model is well fitted to (7) when the hole density is over 10^{19} cm^{-3}, which is particularly important for MOS-based optical modulators. The discrepancy between the modulation efficiency simulated by the Drude model and the Soref's equation (7) is within roughly 20%. We predict that the change in the refractive index of $Si_{0.5}Ge_{0.5}$ will be enhanced relative to that of Si owing to the reduced hole conductivity mass as shown in Fig. 5. The enhancement factor of the change in the refractive index of SiGe relative to that of Si as a function of Ge mole fraction is shown in Fig. 6. The relative change in the refractive index increases with increasing Ge mole fraction, and $Si_{0.5}Ge_{0.5}$ exhibits a three times higher changes in the refractive index than Si.

The free-carrier absorption of compressively strained SiGe on Si was also analyzed by the Drude model. Figure 7 shows the calculated changes in the optical absorption of $Si_{0.5}Ge_{0.5}$ and Si. The hole mobility of SiGe at the acceptor concentration of 3×10^{19} cm^{-3} is assumed in all cases in order to fit the

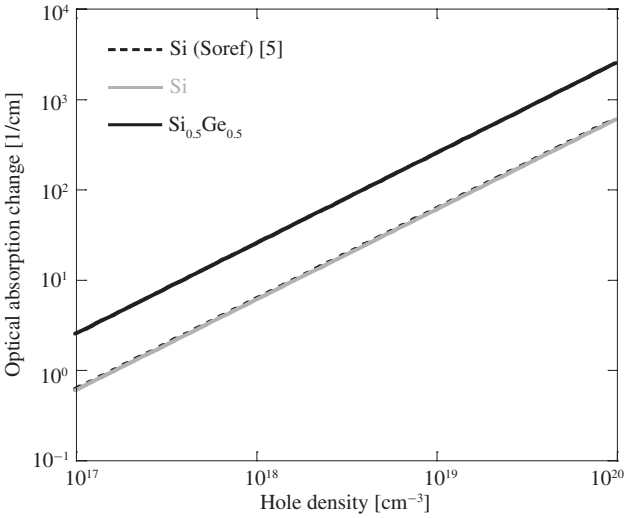

Fig. 7. Changes in optical absorption of compressively strained SiGe and Si calculated by the Drude model. The result for Si obtained from the Soref's model is also plotted as a dotted line.

Drude model of Si to the Soref's model, in which the change in optical absorption is expressed by [5]

$$\Delta\alpha = 8.5 \times 10^{-18}\Delta N_e + 6.0 \times 10^{-18}\Delta N_h. \quad (8)$$

As shown in Fig. 7, the optical absorption of $Si_{0.5}Ge_{0.5}$ is higher than that of Si because of the reduced hole conductivity mass. Figure 8 shows the enhancement factor of the change in optical absorption of compressively strained SiGe relative to that of Si. Since the mobility enhancement of SiGe is slightly less than the value expected from the reduction in hole mass, the enhancement of absorption is slightly larger than that of the refractive index; thus, an enhancement of 4.2 is expected for the free-carrier absorption in the case of $Si_{0.5}Ge_{0.5}$.

III. Analysis of Modulation Characteristics

In Section II, we predicted that the enhancement ratios of 3 and 4.2 in compressively strained $Si_{0.5}Ge_{0.5}$ relative to those

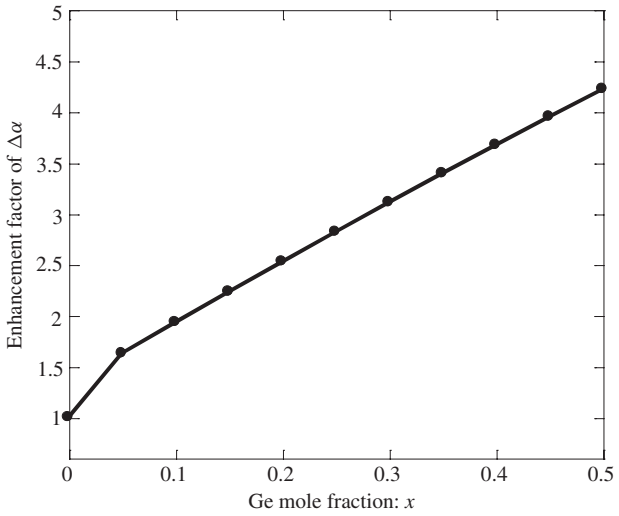

Fig. 8. Enhancement factor of the change in the optical absorption of compressively strained SiGe relative to that of Si as a function of Ge mole fraction.

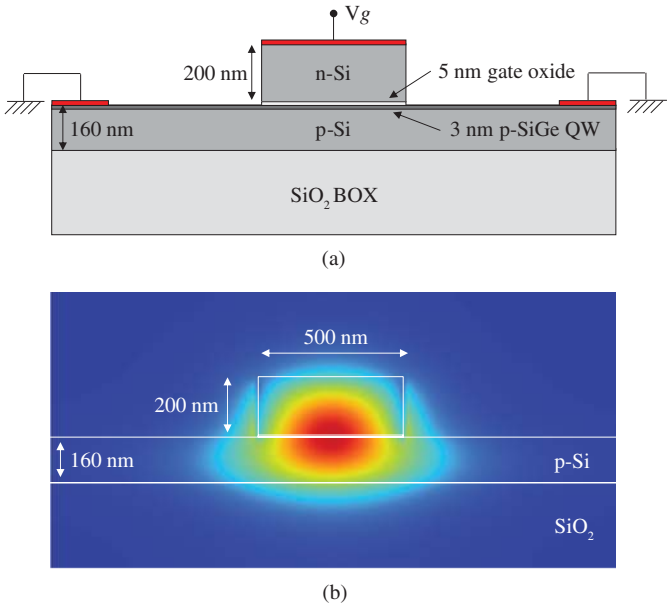

Fig. 9. (a) Cross-sectional schematic of the 3-nm-thick SiGe QW MOS-based optical modulator. (b) Electric field distribution of the fundamental TE mode.

of Si are achievable for the plasma dispersion effect and free-carrier absorption, respectively. In this section, we analyze the modulation characteristics of MOS-based compressively strained SiGe QW optical modulators. An MOS-based modulator uses carrier accumulation at the interface between the gate oxide and the semiconductor, meaning that a SiGe QW with a thickness of a few nanometers is sufficient to confine the carriers that accumulate in the SiGe layer. This feature is suitable for a SiGe-based optical modulator because the epitaxial growth of strained SiGe on Si becomes much easier when the thickness of SiGe is less than its critical thickness [18]. The QW structure is also preferable to the use of SiGe bulk because the energy gap of a SiGe QW is increased by the quantized energy. The energy gap of the 3-nm-thick QW is shown as a gray solid line in Fig. 4, and a quantized energy of 0.12–0.13 eV is predicted. Since the MOS-based optical modulator also enables enhanced modulation efficiency through equivalent oxide thickness (EOT) scaling by high-k dielectrics such as HfO_2 [33], a compressively strained SiGe QW high-k MOS optical modulator is expected to exhibit extremely high modulation efficiency.

A. Simulation Method

The modulation characteristics were analyzed by Synopsys TCAD Sentaurus in conjunction with a finite-difference mode solver for optical waveguides. A cross-sectional schematic of the SiGe QW MOS optical modulator is shown in Fig. 9(a). The MOS diode consists of a 200-nm-thick n-type Si mesa with a doping level of 3×10^{15} cm^{-3}, a 5-nm-thick gate oxide, and a 3-nm-thick p-type SiGe QW grown on a 160-nm-thick p-type silicon-on-insulator (SOI) substrate with a doping level of 1×10^{15} cm^{-3}. The SiGe QW has also been expected to be a high-mobility channel for high-performance pMOSFETs as reported in [34]; thus, the MOS-based modulator structure with a 3-nm-thick SiGe QW can be fabricated by the CMOS-compatible process. We assume the lightly doped Si and SiGe to minimize optical loss, which is not directly related to the modulation efficiency in the simulation. The doping level does not affect the modulation efficiency, although the doping level should be optimized when high-speed operation is considered. We also assume ohmic contact between the metals and semiconductors in the simulation of the modulation characteristics. EOT scaling is taken into account by changing the permittivity of the gate oxide. First, the carrier accumulation upon the application of a gate voltage V_g is simulated by TCAD. Then the changes in the refractive index and absorption of SiGe are calculated by considering the plasma dispersion effect and free-carrier absorption, respectively. Finally, the changes in the phase shift and absorption for the fundamental TE mode shown in Fig. 9(b) are obtained by considering the mode overlap with the SiGe QW. The confinement factor of the SiGe QW is approximately 1.1%, which does not include any slot effects [35] because of the boundary condition of the electric field of the TE mode in the vertical direction. The electrical field of the TE mode is obtained by the finite-difference mode solver.

To verify the accuracy of the simulation method, we simulated the modulation characteristic of the MOS-based Si modulator reported in [12]. We obtained a modulation efficiency of 2.5 V-cm, which is similar to the experimental value of 3.3 V-cm reported in [12]. Although the experimental value might be degraded by many factors such as inferior MOS interfaces, the accuracy of the simulation method is estimated to be within 25%.

B. EOT Scaling Effect

The modulation efficiency of the MOS-based modulator can be enhanced by decreasing the thickness of the gate oxide, which results in an increase in the number of accumulated carriers at the same gate voltage through the increase in the MOS capacitance. However, the scaling of the physical thickness of the gate oxide is limited by the gate leakage current

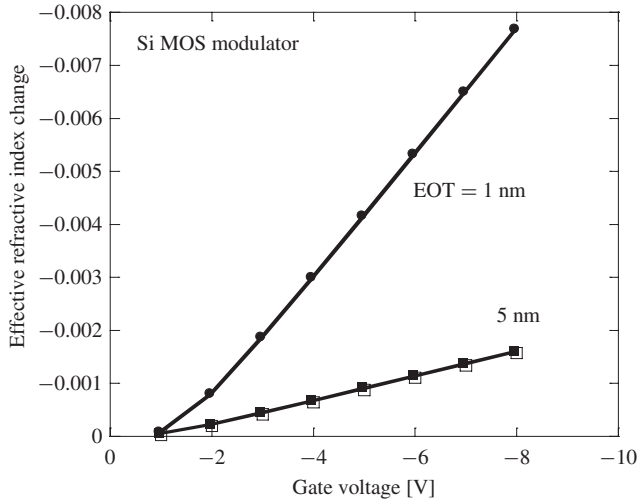

Fig. 10. Changes in effective refractive index of the Si MOS optical modulator with EOTs of 1 nm and 5 nm as a function of gate voltage.

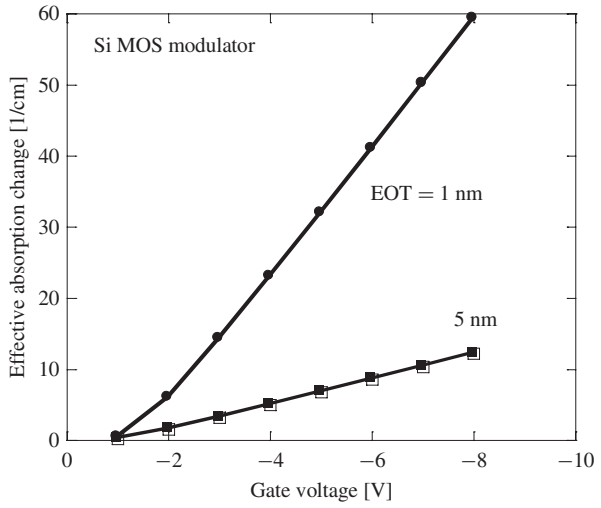

Fig. 11. Changes in effective absorption of the Si MOS optical modulator with EOTs of 1 nm and 5 nm as a function of gate voltage.

through quantum tunneling. In the case of a conventional SiO_2 gate oxide, it is difficult to reduce the thickness to 1 nm. On the other hand, the EOT can be scaled down by increasing the permittivity of the gate oxide while maintaining the same physical thickness. An EOT of approximately 1 nm has already been demonstrated for high-performance Si MOS transistors using a Hf-based high-k dielectric [36]. Thus, a high-k dielectric enables the realization of an MOS-based modulator with an EOT as small as 1 nm.

The calculated changes in the effective refractive index and absorption in the Si MOS modulator for the fundamental TE mode as a function of gate voltage are shown in Figs. 10 and 11, respectively. The changes in the refractive index and absorption linearly increase with the gate voltage swept toward the carrier accumulation. The number of accumulated carriers also linearly increases with the EOT scaling, resulting in increases in the changes in the refractive index and absorption. The accumulated hole concentrations in the p-Si layer underneath the gate oxide for EOTs of 1 nm and 5 nm when the gate voltage is -2 V are shown in Fig. 12. The effect of EOT scaling on the figure of merit for phase modulation, $V_\pi L$, is shown in Fig. 13. In the case of an EOT of 5 nm, a $V_\pi L$ of 0.33 V-cm is obtained, which is one order of magnitude lower than the values in [12] because of the stronger optical confinement as compared with that in [12]. $V_\pi L$ is proportional to the EOT, and a $V_\pi L$ of 0.067 V-cm is predicted for EOT scaling down to 1 nm. We also consider the figure of merit for direct intensity modulation through free-carrier absorption as shown in Fig. 14. The optical loss per unit length for a change in gate voltage of 1 V is proportional to the inverse of the EOT, and an intensity modulation of 4 dB/mm/V is predicted for an EOT of 1 nm.

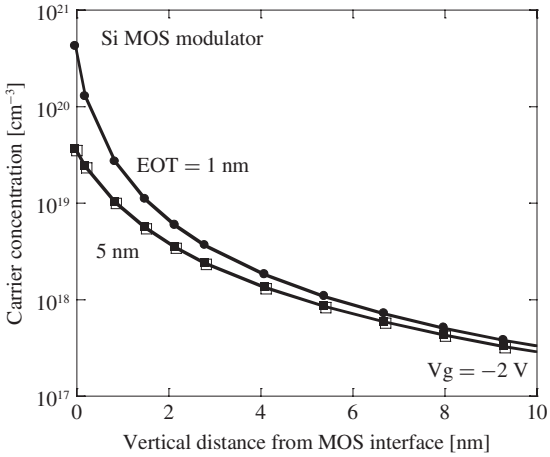

Fig. 12. Hole concentrations in the p-Si layer underneath the gate oxide for EOTs of 1 nm and 5 nm when the gate voltage is -2 V.

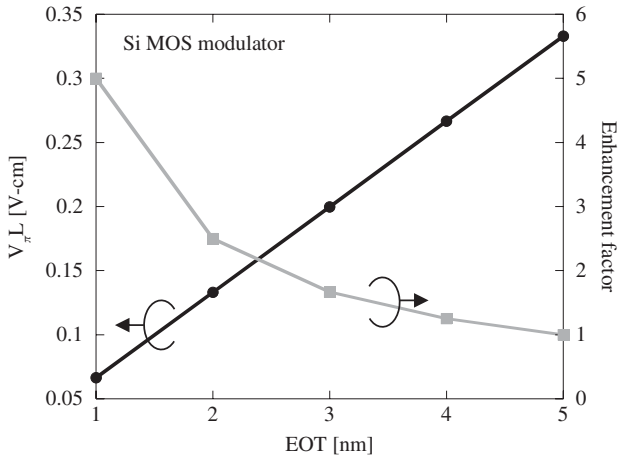

Fig. 13. Effect of EOT scaling on $V_\pi L$ and its enhancement factor relative to that for EOT = 5 nm.

C. SiGe QW High-k MOS Modulator

We analyzed the modulation characteristics of compressively strained SiGe QW high-k MOS optical modulators with an EOT of 1 nm. The changes in the effective refractive index and absorption of the $Si_{0.5}Ge_{0.5}$ QW and Si MOS modulators are shown in Figs. 15 and 16, respectively. As discussed in Section II, the reduction of the hole mass in compressively

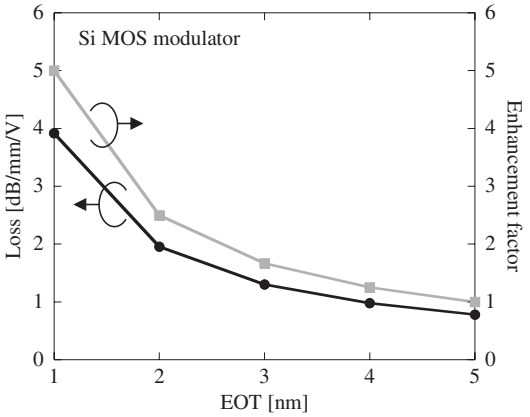

Fig. 14. Effect of EOT scaling on the figure-of-merit for direct intensity modulation and its enhancement factor relative to that for EOT = 5 nm.

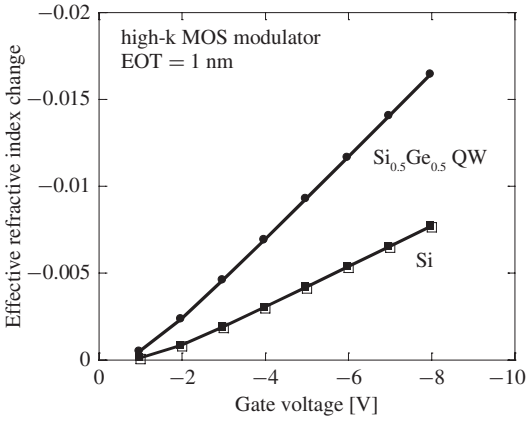

Fig. 15. Changes in effective refractive index of the compressively strained SiGe QW and Si high-k MOS optical modulators with EOTs of 1 nm.

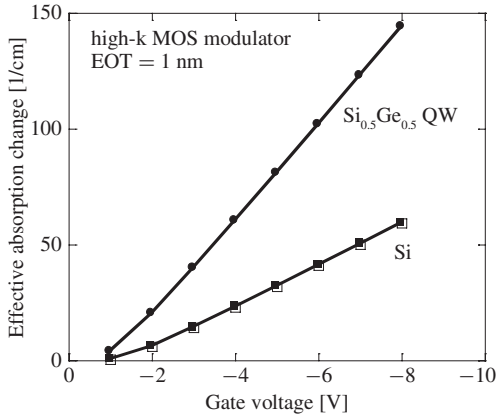

Fig. 16. Changes in effective absorption of the compressively strained SiGe QW and Si high-k MOS optical modulators with EOTs of 1 nm.

strained SiGe enhances the modulation efficiency relative to that of Si. Linear modulation characteristics in the refractive index and absorption are obtained even in the 3-nm-thick QW modulator because the accumulated holes are effectively confined to the interface between SiGe and the gate oxide. The modulation efficiencies of the SiGe QW MOS modulators as a function of Ge mole fraction are shown in Figs. 17 and 18.

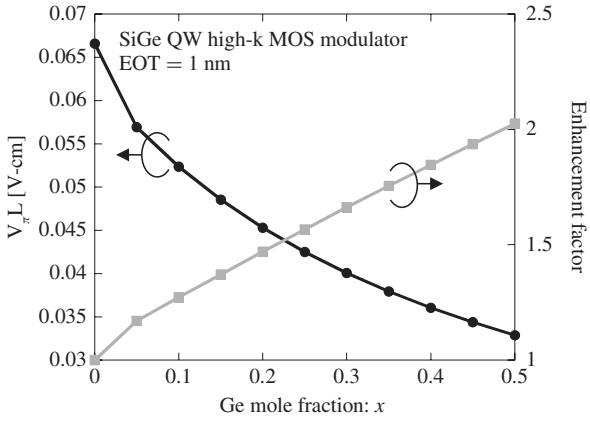

Fig. 17. $V_\pi L$ of SiGe QW MOS modulator with an EOT of 1 nm and its enhancement factor relative to that of Si as a function of Ge fraction.

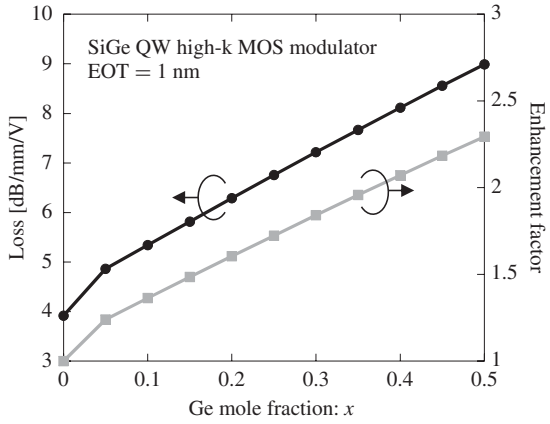

Fig. 18. Optical loss per unit length for a 1 V change in gate voltage of SiGe QW MOS modulator with an EOT of 1 nm and its enhancement factor relative to that of Si as a function of Ge fraction.

As shown in Fig. 17, the phase modulation efficiency increases with increasing Ge mole fraction through hole mass modulation, and twice the enhancement as compared with that for Si is obtained for a Ge mole fraction of up to 0.5. The enhancement factor of the phase modulation is lower than that for the SiGe bulk shown in Fig. 6 because there is no enhancement in the plasma dispersion effect induced through the accumulated electrons in the n-Si mesa. However the hole mass modulation by employing compressive strain in conjunction with EOT scaling from 5 nm to 1 nm enables an approximately 10-fold enhancement in the phase modulation efficiency. The $Si_{0.5}Ge_{0.5}$ QW high-k MOS optical modulator with an EOT of 1 nm is predicted to exhibit an extremely small $V_\pi L$ of 0.033 V-cm, which is more than 10 times smaller than the reported value for a Si MOS modulator with an EOT of 5 nm [37]. The enhancement factor of the change in the optical loss per unit length for a 1 V change in gate voltage shown in Fig. 18 is slightly larger than that of the change in the refractive index predicted in Fig. 17. The enhancement of direct intensity modulation efficiency reaches 2.3 for a Ge mole fraction of up to 0.5, and an intensity modulation of 9 dB/mm/V is predicted. The efficiency of intensity modulation is more than 10 times as large as the predicted value for the Si MOS modulator with

EOT = 5 nm; therefore, the use of high-Ge-content SiGe and EOT scaling down to 1 nm should enable the realization of a direct intensity modulator through free-carrier absorption with a much simpler and more compact structure than an MZI-based modulator.

IV. Conclusion

The strain engineering of SiGe optical modulators was discussed with the aim of enhancing the plasma dispersion effect and free-carrier absorption. Compressively strained $Si_{0.5}Ge_{0.5}$ grown on Si was predicted to have a three times higher plasma dispersion effect and four times higher free carrier absorption than Si through the reduction of the hole conductivity mass. We predicted that a $Si_{0.5}Ge_{0.5}$ quantum well high-k MOS optical modulator will exhibit an extremely small $V_\pi L$ of 0.033 V-cm in conjunction with EOT scaling down to 1 nm. The efficiency of direct intensity modulation was also predicted to be 9 dB/mm/V, which makes an intensity modulator based on free-carrier absorption feasible. Strain engineering is currently an essential technology for enhancing the performance of Si MOS transistors and is also promising for enhancing the performance of optical modulators through conductivity mass modulation.

Acknowledgment

The authors would like to thank Y. Kamakura of Osaka University, Osaka, Japan, and K. Takeda of NTT Photonics Laboratory, Japan, for support in the $k \cdot p$ method for the SiGe band analysis and finite-difference waveguide mode analysis.

References

[1] G. T. Reed, G. Mashanovich, F. Y. Gardes, and D. J. Thomson, "Silicon optical modulators," *Nat. Photon.*, vol. 4, pp. 518–526, Jul. 2010.

[2] A. Liu, R. Jones, L. Liao, D. Samara-Rubio, D. Rubin, O. Cohen, R. Nicolaescu, and M. Paniccia, "A high-speed silicon optical modulator based on a metal-oxide-semiconductor capacitor," *Nature*, vol. 427, pp. 615–618, Feb. 2004.

[3] J. Liu, M. Beals, A. Pomerene, S. Bernardis, R. Sun, J. Cheng, L. C. Kimerling, and J. Michel, "Waveguide-integrated, ultralow-energy GeSi electro-absorption modulators," *Nat. Photon.*, vol. 2, pp. 433–437, May 2008.

[4] Y. H. Kuo, Y. K. Lee, Y. Ge, S. Ren, J. E. Roth, T. I. Kamins, D. A. B. Miller, and J. S. Harris, "Strong quantum-confined Stark effect in germanium quantum-well structures on silicon," *Nature*, vol. 437, pp. 1334–1336, Oct. 2005.

[5] R. A. Soref and B. R. Bennett, "Electrooptical effects in silicon," *IEEE J. Quantum Electron.*, vol. 23, no. 1, pp. 123–129, Jan. 1987.

[6] C. Gunn, "CMOS photonics for high-speed interconnects," *IEEE Micro*, vol. 26, no. 2, pp. 58–66, Mar.–Apr. 2006.

[7] A. Liu, L. Liao, D. Rubin, H. Nguyen, B. Ciftcioglu, Y. Chetrit, N. Izhaky, and M. Paniccia, "High-speed optical modulation based on carrier depletion in a silicon waveguide," *Opt. Exp.*, vol. 15, no. 2, pp. 660–668, 2007.

[8] L. Liao, A. Liu, D. Rubin, J. Basak, Y. Chetrit, H. Nguyen, R. Cohen, N. Izhaky, and M. Paniccia, "40 Gbit/s silicon optical modulator for high speed applications," *Electron. Lett.*, vol. 43, no. 22, pp. 1196–1197, Oct. 2007.

[9] N. N. Feng, S. Liao, D. Feng, P. Dong, D. Zheng, H. Liang, R. Shafiiha, G. Li, J. E. Cunningham, A. V. Krishnamoorthy, and M. Asghari, "High speed carrier-depletion modulators with 1.4V-cm $V_\pi L$ integrated on 0.25 μm silicon-on-insulator waveguides," *Opt. Exp.*, vol. 18, no. 8, pp. 7994–7999, 2010.

[10] M. R. Watts, W. A. Zortman, D. C. Trotter, R. W. Young, and A. L. Lentine, "Low-voltage, compact depletion-mode, silicon Mach-Zehnder modulator," *IEEE J. Select. Topics Quantum Electron.*, vol. 16, no. 1, pp. 159–164, Jan.–Feb. 2010.

[11] F. Y. Gardes, D. J. Thomson, N. G. Emerson, and G. T. Reed, "40 Gb/s silicon photonics modulator for TE and TM polarizations," *Opt. Exp.*, vol. 19, no. 12, pp. 11804–11814, 2011.

[12] L. Liao, D. Samara-Rubio, M. Morse, A. Liu, D. Hodge, D. Rubin. U. D. Keil, and T. Franck, "High speed silicon Mach-Zehnder modulator," *Opt. Exp.*, vol. 13, no. 8, pp. 3129–3135, Apr. 2005.

[13] L. Liao, A. Liu, R. Jones, D. Rubin, D. Samara-Rubio, O. Cohen, M. Salib, and M. Paniccia, "Phase modulation efficiency and transmission loss of silicon optical phase shifters," *IEEE J. Quantum Electron.*, vol. 41, no. 2, pp. 250–257, Feb. 2005.

[14] X. Zheng, J. Lexau, Y. Luo, H. Thacker, T. Pinguet, A. Mekis, G. Li, J. Shi, P. Amberg, N. Pinckney, K. Raj, R. Ho, J. E. Cunningham, and A. Krishnamoorthy, "Ultralow-energy all-CMOS modulator integrated with driver," *Opt. Exp.*, vol. 18, no. 3, pp. 3059–3070, Feb. 2010.

[15] Q. Xu, B. Schmidt, S. Pradhan, and M. Lipson, "Micrometre-scale silicon electro-optic modulator," *Nature*, vol. 435, pp. 325–327, May 2005.

[16] Q. Xu, S. Manipartruni, B. Schmidt, J. Shakya, and M. Lipson, "12.5 Gbit/s carrier-injection-based silicon micro-ring silicon modulators," *Opt. Exp.*, vol. 15, no. 2, pp. 430–436, Jan. 2007.

[17] W. M. Green, M. J. Rooks, L. Sekaric, and Y. A. Vlasov, "Ultracompact, low RF power, 10 Gb/s silicon Mach-Zehnder modulator," *Opt. Exp.*, vol. 15, no. 25, pp. 17106–17113, 2007.

[18] R. People and J. C. Bean, "Calculation of critical layer thickness versus lattice mismatch for Ge_xSi_{1-x}/Si strained-layer heterostructures," *Appl. Phys. Lett.*, vol. 47, no. 3, pp. 322–324, Aug. 1985.

[19] M. M. Rieger and P. Vogl, "Electronic-band parameters in strained $Si_{1-x}Ge_x$ alloys on $Si_{1-y}Ge_y$ substrates," *Phys. Rev. B*, vol. 48, no. 19, pp. 14276–14287, 1993.

[20] J. M. Luttinger and W. Kohn, "Motion of electrons and holes in perturbed periodic fields," *Phys. Rev.*, vol. 97, no. 4, pp. 869–883, 1955.

[21] J. M. Luttinger, "Quantum theory of cyclotron resonance in semiconductors: General theory," *Phys. Rev.*, vol. 102, no. 4, pp. 1030–1041, 1956.

[22] C. Y. P. Chao and S. L. Chuang, "Spin-orbit-coupling effects on the valence-band structure of strained semiconductor quantum wells," *Phys. Rev. B*, vol. 46, no. 7, pp. 4110–4122, 1992.

[23] P. Y. Yu and M. Cardona, *Fundamentals of Semiconductors*. New York: Springer-Verlag, 1995.

[24] Y. Shiraki and N. Usami, *Silicon-Germanium (SiGe) Nanostructures*. Cambridge, U.K.: Woodhead Publishing, 2011.

[25] M. V. Fischetti and S. E. Laux, "Band structure, deformation potentials, and carrier mobility in strained Si, Ge, and SiGe alloys," *J. Appl. Phys.*, vol. 80, no. 4, pp. 2234–2252, 1996.

[26] J. P. Dismukes, L. Ekstrom, and R. J. Paff, "Lattice parameter and density in germanium silicon alloys," *J. Phys. Chem.*, vol. 68, no. 10, pp. 3021–3027, 1964.

[27] B. R. Bennett, R. A. Soref, and J. A. D. Alamo, "Carrier-induced change in refractive index of InP, GaAs, and InGaAsP," *IEEE J. Quantum Electron.*, vol. 26, no. 1, pp. 113–122, Jan. 1990.

[28] T. Manku, J. M. McGregor, A. Nathan, D. J. Roulston, J. P. Noel, and D. C. Houghton, "Drift hole mobility in strained and unstrained doped $Si_{1-x}Ge_x$ alloys," *IEEE Trans. Electron. Dev.*, vol. 40, no. 11, pp. 1990–1996, Nov. 1993.

[29] N. D. Arora, J. R. Hauser, and D. J. Roulston, "Electron and hole mobilities in silicon as a function of concentration and temperature," *IEEE Trans. Electron. Dev.*, vol. 29, no. 2, pp. 292–295, Feb. 1982.

[30] D. V. Lang, R. People, J. C. Bean, and A. M. Sergent, "Measurement of the band gap of Ge_xSi_{1-x}/Si strained-layer heterostructures," *Appl. Phys. Lett.*, vol. 47, no. 12, pp. 1333–1335, Dec. 1985.

[31] D. J. Robbins, L. T. Canham, S. J. Barnett, A. D. Pitt, and P. Calcott, "Near-band-gap photoluminescence from pseudomorphic $Si_{1-x}Ge_x$ single layers on silicon," *J. Appl. Phys.*, vol. 71, no. 3, pp. 1407–1414, Feb. 1992.

[32] F. Schaffler, *Properties of Advanced Semiconductor Materials GaN, AlN, InN, BN, SiC, SiGe*. New York: Wiley, 2001.

[33] L. Manchanda, M. L. Green, R. B. van Dover, M. D. Morris, A. Kerber, Y. Hu, J. P. Han, P. J. Silverman, T. W. Sorsch, G. Weber, V. Donnelly, K. Pelhos, F. Klemens, N. A. Ciampa, A. Kornblit. Y. O. Kim, J. E. Bower, D. Barr, E. Ferry, D. Jacobson, J. Eng, B. Busch, and H. Schulte, "Si-doped aluminates for high temperature metal-gate CMOS: Zr-Al-Si-O, a novel gate dielectric for low power applications," in *Proc. Electron Dev. Meeting Tech. Dig. Int.*, San Francisco, CA, 2000, pp. 23–26.

[34] G. Hellings, L. Witters, R. Krom, J. Mitard, A. Hikavyy, R. Loo, A. Schulze, G. Eneman, C. Kerner, J. Franco, T. Chiarella, S. Takeoka, J. Tseng, W. Wang, W. Vandervorst, P. Absil, S. Biesemans, M. Heyns, K. De Meyer, M. Meuris, and T. Hoffmann, "Implant-free SiGe quantum well pFET: A novel, highly scalable and low thermal budget device, featuring raised source/drain and high-mobility channel," in *Proc. IEEE Electron Dev. Meeting Int. Tech. Dig.*, San Francisco, CA, 2010, pp. 10.4-1–10.4-4.

[35] V. R. Almeida, Q. Xu, C. A. Barrios, and M. Lipson, "Guiding and confining light in void nanostructure," *Opt. Lett.*, vol. 29, no. 11, pp. 1209–1211, 2004.

[36] K. Mistry, C. Allen, C. Auth, B. Beattie, D. Bergstrom, M. Bost, M. Brazier, M. Buehler, A. Cappellani, R. Chau, C.-H. Choi, G. Ding, K. Fischer, T. Ghani, R. Grover, W. Han, D. Hanken, M. Hattendorf, J. He, J. Hicks, R. Huessner, D. Ingerly, P. Jain, R. James, L. Jong, S. Joshi, C. Kenyon, K. Kuhn, K. Lee, H. Liu, J. Maiz, B. McIntyre, P. Moon, J. Neirynck, S. Pae, C. Parker, D. Parsons, C. Prasad, L. Pipes, M. Prince, P. Ranade, T. Reynolds, J. Sandford, L. Shifren, J. Sebastian, J. Seiple, D. Simon, S. Sivakumar, P. Smith, C. Thomas, T. Troeger, P. Vandervoorn, S. Williams, and K. Zawadzki, "A 45 nm logic technology with high-k^{+} metal gate transistors, strained silicon, 9 Cu interconnect layers, 193 nm dry patterning, and 100% Pb-free Packing," in *Proc. IEEE Electron Dev. Meeting Int. Tech. Dig.*, Dec. 2007, pp. 247–250.

[37] J. Fujikata, J. Ushida, Y. Ming-Bin, Z. S. Yang, D. Liang, P. L. Guo-Qiang, D. L. Kwong, and T. Nakamura, "25 GHz operation of silicon optical modulator with projection MOS structure," in *Proc. Collocated Nat. Fiber Opt. Eng. Conf. Opt. Fiber Commu.*, San Diego, CA, 2010, pp. 1–3.

Mitsuru Takenaka (M'02) was born in Kobe, Japan, in 1975. He received the B.E., M.E., and Ph.D. degrees in electronic engineering from the University of Tokyo, Tokyo, Japan, in 1998, 2000, and 2003, respectively.

He was a Research Fellow with the Optoelectronics Industry and Technology Development Association, Washington D.C., from 2003 to 2007, where he was engaged in research on photonic routers. In 2007, he joined the Department of Electrical Engineering, University of Tokyo, as a Lecturer. Since 2008, he has been an Associate Professor with the Department of Electrical Engineering and Information Systems, University of Tokyo. His current research interests include heterogeneous integration for III–V/Ge complementary metal-oxide semiconductor (CMOS) transistors and III–V/Si CMOS photonics.

Dr. Takenaka is a member of the IEEE Photonics Society, the IEEE Electron Devices Society, the Institute of Electronics, Information, and Communication Engineers (IEICE), and the Japan Society of Applied Physics (JSAP). He received the Young Scientist Award for the Presentation of an Excellent Paper from JSAP in 2003 and the Young Researchers' Award from IEICE in 2005.

Shinichi Takagi (M'93) was born in Tokyo, Japan, on August 25, 1959. He received the B.S., M.S., and Ph.D. degrees in electronic engineering from the University of Tokyo, Tokyo, in 1982, 1984, and 1987, respectively.

He joined Toshiba Research and Development Center, Kawasaki, Japan, in 1987, where he was engaged in research on the device physics of Si metal-oxide-semiconductor field-effect transistors (MOSFETs), including carrier transport in the inversion layers, impact ionization phenomena, hot carrier degradation, and the electric properties of Si/SiO_2 interfaces. From 1993 to 1995, he was a Visiting Scholar with Stanford University, Stanford, CA, where he studied Si/SiGe heterostructure devices. He was on the MIRAI Project as the Leader of the Ultra-High Performance New Transistor Structures Theme from 2001 to 2007. In October 2003, he moved to the University of Tokyo, where he is currently a Professor with the Department of Electrical Engineering and Information Systems, School of Engineering. His current research interests include the science and technology of advanced complementary metal-oxide semiconductor devices including new-channel-material MOSFETs based on strained Si, Ge, and III–Vs.

Dr. Takagi has served on the technical program committees of several international conferences including the International Electron Devices Meeting, the Symposium on Very Large Scale Integration Technology, the International Reliability Physics Symposium, the International Conference on Solid State Devices and Materials, and the International Solid State Circuits Conference. He is a member of the IEEE Electron Device Society and the Japan Society of Applied Physics.